Topology optimization of thermoelectric generator for maximum power efficiency

Jungsoo Lee[1†], Seong Eun Yang[1†], Seungjun Choo[1†] Haiyang Li[1], Hyunjin Han[1], Ke onkuk Kim[1], Yae Eun Park[1], Hayoung Chung[2*], and Jae Sung Son[1*]

[1]*Department of Chemical Engineering, Pohang University of Science and Technology (POSTECH), Gyeongsangbuk-do, 37673, Republic of Korea.*

[2]*Department of Mechanical Engineering, Ulsan National Institute of Science and Technology (UNIST), Ulsan, 44919, Republic of Korea.*

[†]*These authors contributed equally to this work.*

Correspondences to: hychung@unist.ac.kr (H.C.), & sonjs@postech.ac.kr (J.S.S.)

This supplement contains

Supplementary discussion

Supplementary Figures 1-10

Introduction

This document contains Supplementary Information pertinent to the main draft. The topics addressed are:

(1) Optimums with different contact resistivities

(2) Optimums with different aspect ratios

(3) Optimums with different load resistances

(4) Optimums with different objective functions

(5) Optimums with different material properties under fixed temperature condition

Optimums with different contact resistivities

Contact resistance at the metal-semiconductor junction is unavoidable and sometimes critically affects the overall device efficiency[1,2]. As well, we identified that contact resistance at the interface between the electrodes and the TE material is also among the key system parameters that strongly influence power-generating efficiency. We performed an optimization study by varying the contact resistivity (ρ_c) (Extended Data Fig. 5a). At lower ρ_c values, the optimal geometry approaches a cylindrical geometry. As ρ_c increases, the contact area expands, increasing both the improvement of efficiency and the volume of the optimal geometry. This trend is in contrast to the previous boundary conditions cases. The geometry transitions toward a more pronounced I-shape, with a narrower central cross-section than that observed at lower ρ_c. The R_{th} of the optimized geometry rises sharply due to its narrower cross-section, yielding nearly a twofold greater ΔT and a marked increase in the $\mathcal{E}$ compared to the cuboid. In other words, the conversion factor is enhanced by optimal design (Extended Data Fig. 5e). From the perspective of matching conductance, when ρ_c is relatively low, there is little difference between the optimized geometry and the cuboid shape. However, as ρ_c becomes larger, that difference grows accordingly. Beyond a certain threshold, the gap in matching conductance between the cuboid and optimized designs begins to narrow, so the advantage gained from shape control primarily arises through improvements in the conversion factor. This finding suggests that, in designing TE materials, different strategies may be required depending on the magnitude of ρ_c .

Optimums with different aspect ratios

The aspect ratio is a fundamental geometric parameter that dictates the relative proportions of a TE leg in the height and cross-sectional directions. A high aspect ratio can increase the temperature difference across the leg but may also lead to excessive electrical resistance. Conversely, a low aspect ratio might reduce the temperature gradient. Therefore, careful modulation of the aspect ratio permits optimization of the trade-off between the temperature gradient and electrical resistance, thereby enhancing TE generation efficiency[3,4]. In this study, the evolution of the optimal geometry was examined by combining aspect ratio variation with TO, thereby introducing additional shape degrees of freedom. The findings reveal that a decrease in the aspect ratio leads to a greater enhancement in TE efficiency, while the volume fraction relative to the design domain remains nearly constant (Extended Data Fig. 5b). This improvement arises because the TO framework redistributes material to maintain an effective path for both heat and electrical flows. Moreover, while the optimized geometries converge to similar values of conversion factor and matching conductance regardless of aspect ratio, cuboid references exhibit more scattered performance (Extended Data Fig. 5f). In particular, small-aspect-ratio cuboids display higher matching conductance at the cost of a notably lower conversion factor, diminishing overall efficiency. Through TO, we were able to enhance the initially low conversion factor by approximately 12-fold while reducing matching conductance by about 3.5-fold, thereby tripling the efficiency. The results of this study indicate that TE leg geometries can be effectively optimized to conform to the spatial constraints typical of restricted TE generator applications.

Optimums with different load resistances

Load resistance is critical in TE applications because it determines how effectively the internal electrical conduction of the device couples with the external circuit. If the load is too small, the current can be too high, resulting in suboptimal voltage and power. If the load is too large, the voltage might be higher but overall power output drops due to reduced current. Therefore, when TE power generation is applied in practical settings, load resistance becomes a key parameter that ultimately determines the overall conversion efficiency[5,6]. To observe the effect of load resistance in an optimal geometry, we performed TO by varying load resistance (Extended Data Fig. 5c). Results indicate that as load resistance increases, the performance gap between the optimized design and the cuboid widens: the optimized geometry attains greater efficiency gains. Critically, our results show that for higher load resistances, the gain in conversion factor outweighs the drop in matching conductance, yielding substantial efficiency improvements (Extended Data Fig. 5g). This outcome highlights how TO solutions can dynamically adapt to different load conditions in a way that simple cuboid geometries cannot, thereby maximizing efficiency in real-world TE systems where load characteristics frequently vary.

Optimums with different objective functions

In TE design, the choice of objective function—whether to maximize total power output or conversion efficiency—directly shapes how heat and electricity flow within the device. Many applications prioritize absolute power (for instance, to supply electricity in remote locations[7,8]), while others prize energy efficiency (e.g., to recapture waste heat with minimal loss). By assigning different objective functions within the TO process, we found that power-maximized optimizations substantially boost matching conductance, thus increasing current flow and net output power (Extended Data Fig. 5d). However, these designs might not fully harness the available heat. In contrast, optimizing for efficiency tends to enhance both the matching conductance and the conversion factor, resulting in a more balanced utilization of thermal energy (Extended Data Fig. 5h). The resulting geometries feature carefully shaped cross-sections that maintain a strong temperature difference while also ensuring adequate electrical conduction. Notably, our findings reveal that even a small shift in the objective—from maximizing power to maximizing efficiency—can yield a markedly different final geometry, underscoring the versatility and responsiveness of TO as a design tool. This adaptability is especially relevant when TE systems operate under diverse environmental conditions or mission requirements, reinforcing the notion that a single “best” shape does not exist independently of the chosen design goal.

Optimums with different material properties under fixed temperature condition

We performed the TO under fixed temperature conditions (hot side at 500 K, cold side at 323 K) for nine different TE materials (Extended Data Fig. 7). The resulting optimal geometries fell into two categories: some used the maximum allowable material volume, while others markedly reduced the volume to form a pronounced "I" shape. Materials like BiSbTe, AgCuTe, and MgAgSb, which achieve their peak *ZT* in this temperature range, retained the maximum material volume, resulting in less than 1% performance difference compared to a simple cuboid (Extended Data Fig. 7b,c). Although Cu_2Se does not reach its highest *ZT* under these conditions, its intrinsically low thermal conductivity yields a modest input Q_h, prompting the design to favor maximizing electrical transport rather than further reducing Q_h through shape control—thus it also uses the maximum volume. In contrast, PbTe, GeTe, ZrNiSn, and FeNbSb substantially cut down their material volume, giving rise to an "I" shape. By pushing the R_m to its peak and increasing the R_{el}, these geometries reduce their matching conductance, thereby boosting their conversion factor (Extended Data Fig. 7d). As a result, FeNbSb exhibits more than a 200% gain in efficiency. In short, under fixed temperature conditions, materials with high electrical conductivity can achieve improved energy conversion efficiency by tailoring geometry to maximize the R_m and reduce Q_h through increased R_{th}. In addition, materials with relatively high thermal conductivity benefit from shape control that minimizes the absolute Q_h, thereby further enhancing efficiency.

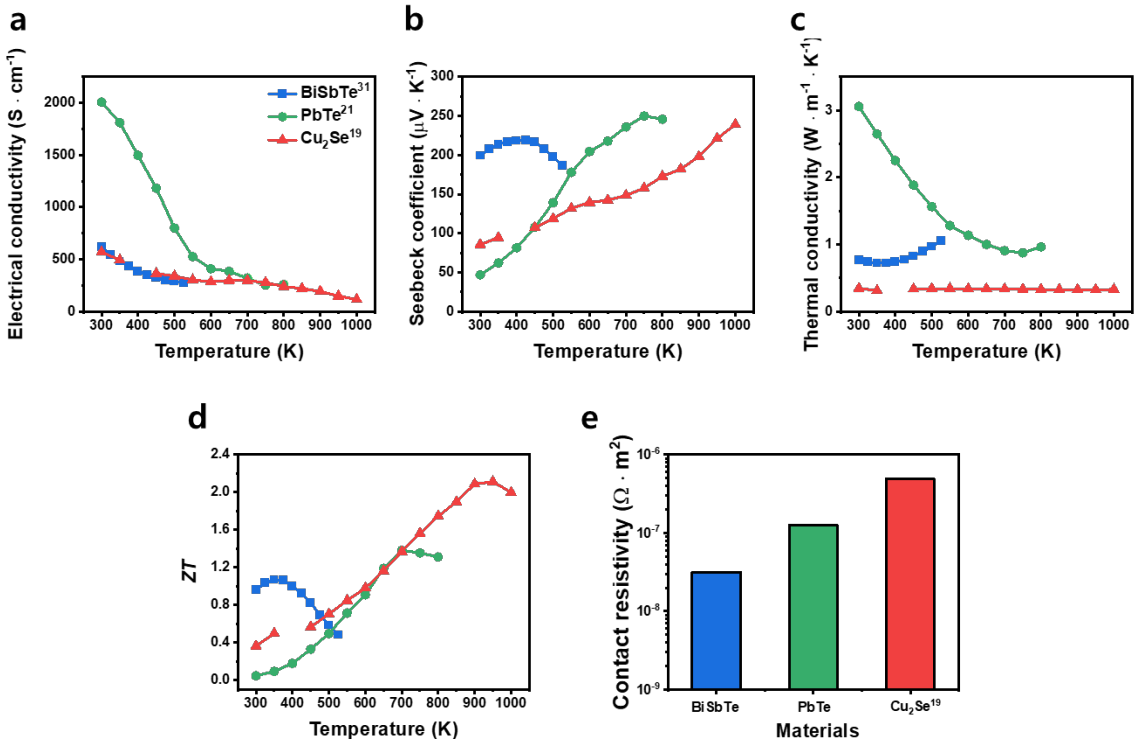

Supplementary Fig. 1 | Thermoelectric properties and contact resistivity. a–d, Temperature-dependent electrical conductivities (**a**), Seebeck coefficients (**b**), thermal conductivities (**c**) and *ZT* (**d**) of the 3D printed BiSbTe, PbTe and Cu_2Se. **e**, The measured contact resistivity of 3D printed BiSbTe, PbTe and Cu_2Se. Material properties were adopted from Ref. 19, 21 and 31.

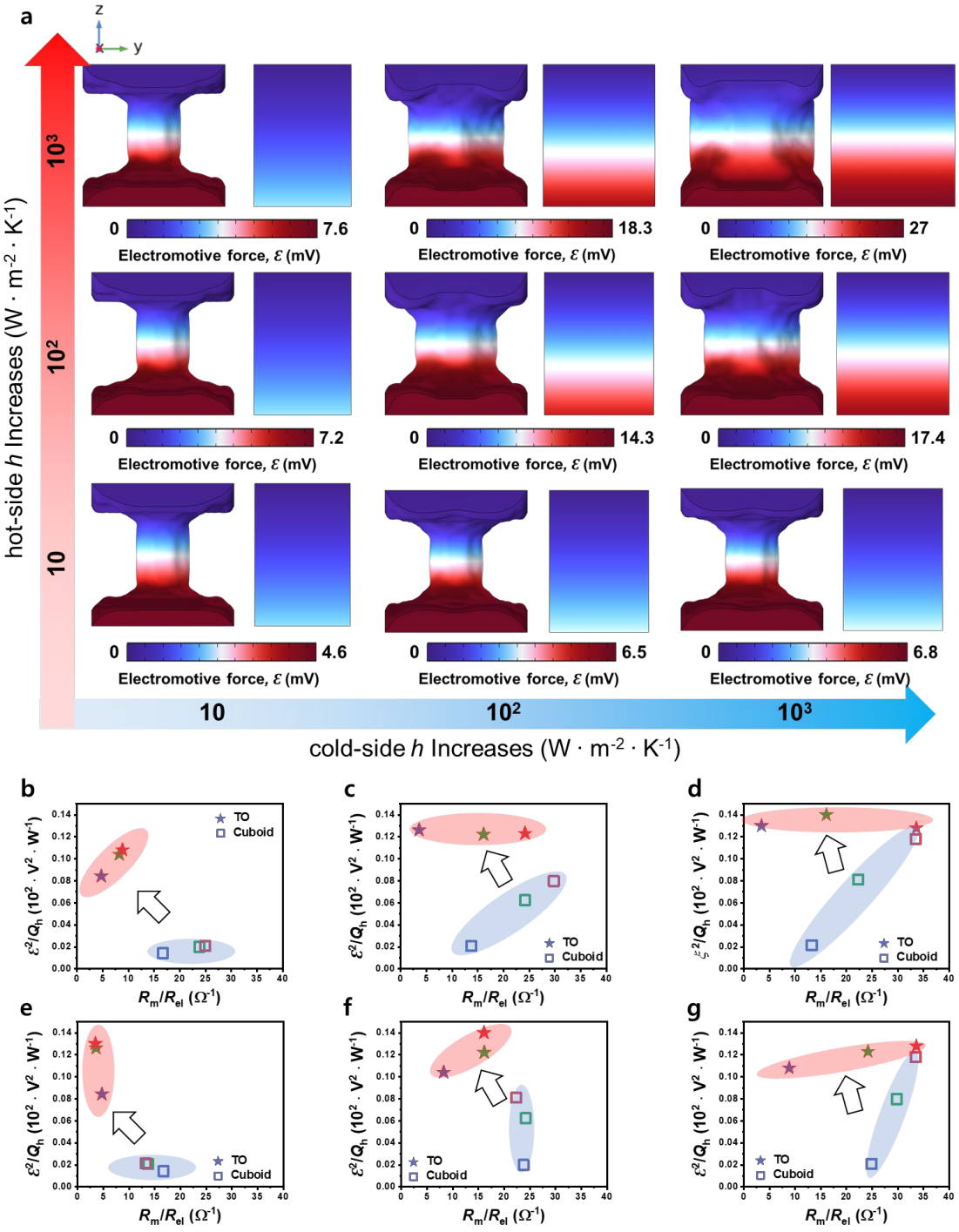

Supplementary Fig. 2 | TO under convective cooling and heating. a, Side views of the electromotive force distribution in optimized BiSbTe geometries under convective cooling and heating conditions, with h varied from10 to10^3 W m^{-2} K^{-1}.**b**–**g**, Evaluation of the η enhancemen through optimal design from the perspectives of conversion factor and matching conductance when the cold-side h is varied (**b**–**d**) at a fixed hot-side h of 10 (**b**), 10^2 (**c**) and 10^3 (**d**) W m^{-2} K^{-1} and when the hot-side h is varied (**e**–**g**) at a fixed cold-side h of 10 (**e**), 10^2 (**f**) and 10^3 (**g**) W m^{-2} K^{-1} . Blue denotes the lowest h, green intermediate, and red the highest. The star shape denotes the optimal geometries, and the hollow square denotes the cuboid geometry.

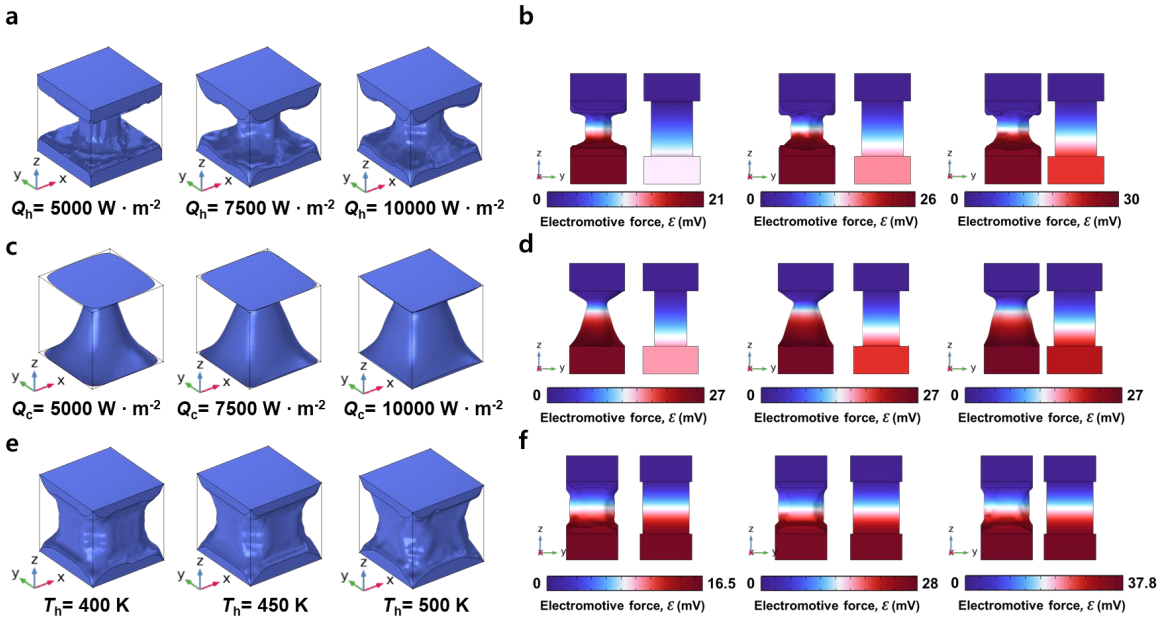

Supplementary Fig. 3 | TO under different thermal boundaries . a,**c**,**d**, Optimal designs for different Q_h and convective cooling (**a**), a fixed T_h with varying Q_c (**c**), and a range of fixed ΔT (**d**). **b**,**d**,**f**, Electromotive force distributions for each optimal design (left) compared with a reference cuboid of same volume (right). Specifically, **b** corresponds to **a**, **d** to **c**, and **f** to **d**.

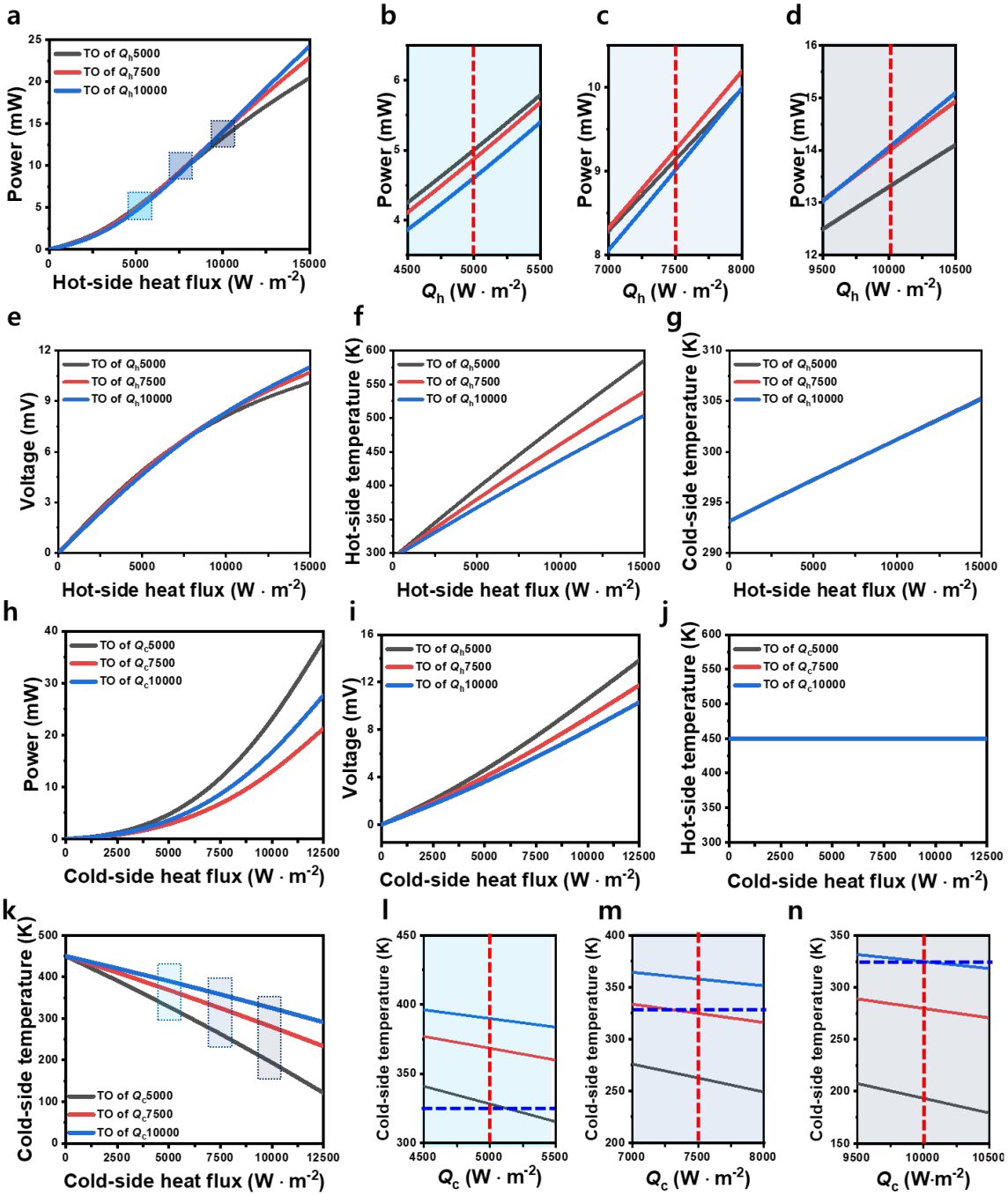

Supplementary Fig. 4 | Evaluation of optimial design by numerical simulations. a–g, Numerical results of optimal design under a fixed Q_h and convective cooling with h=1200 W m^{-2} K^{-1}. Panels show output power (**a**–**d**), voltage (**e**), T_h (**f**) and T_c (**g**). The areas labeled in panel **a** correspond to panels **b**, **c**, and **d**, respectively. **h**–**n**, Numerical results of optimal design under a fixed T_h of 450 K and fixed Q_c. Panels **h** and **i** show output power and voltage, respectively, while **j** shows hot-side temperature and **k**–**n** show T_c. The vertical red dashed lines indicate the optimal points, and the horizontal blue dashed lines denote the pre-set temperature limit. The areas labeled in panel **k** correspond to panels **l**, **m**, and **n**, respectively.

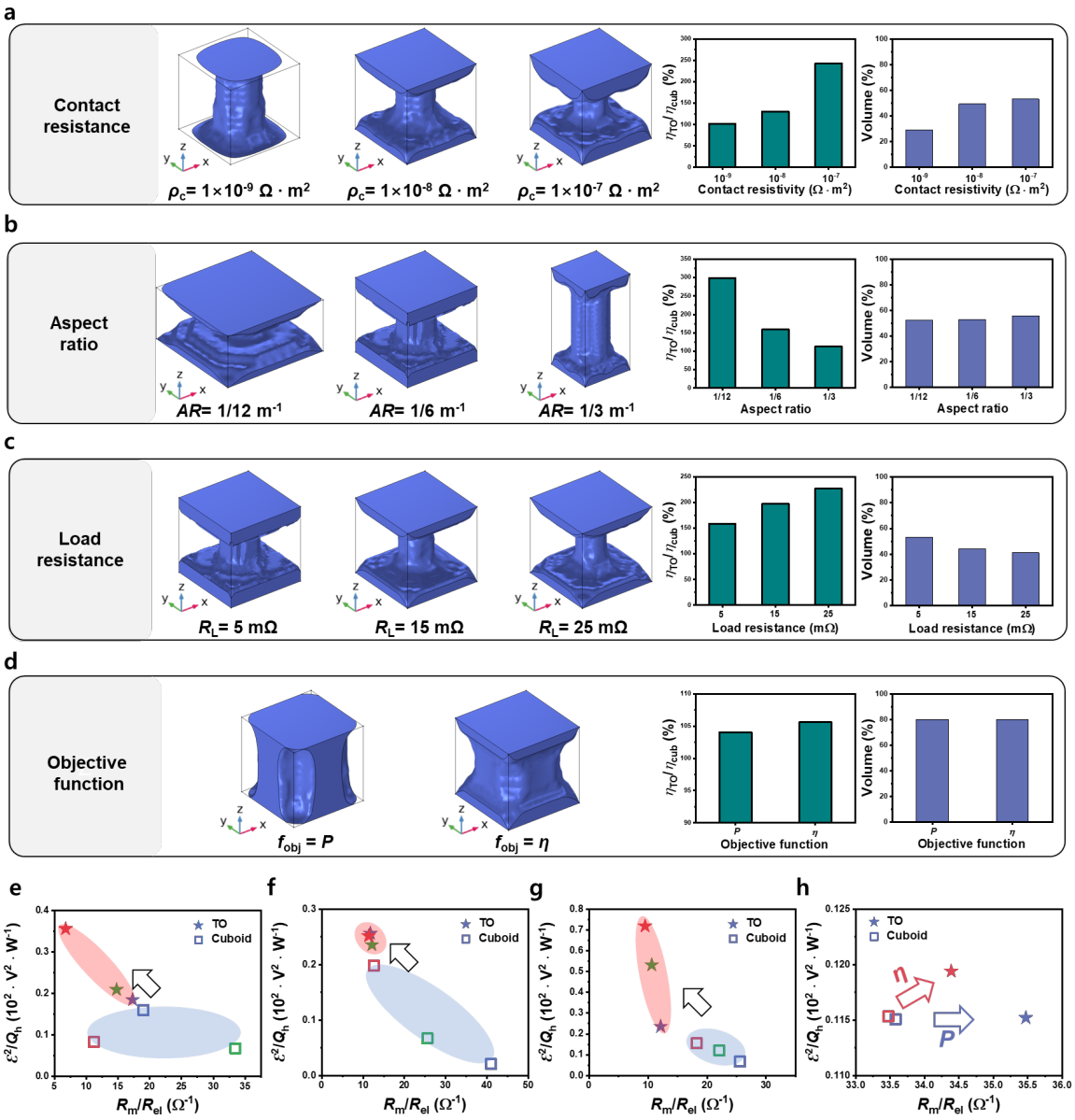

Supplementary Fig. 5 | TO under different system parameters. a–d, The optimized geometries of BiSbTe model under different system parameters such as contact resistivity (**a**), aspect ratio (**b**), load resistance (**c**) and objective function (**d**). **j–l**, Analysis of the η enhancement achieved through optimal design from **a** (**e**), from **b** (**f**), from **c** (**g**) and from **d** (**h**). Blue indicates the lowest system parameter values, green indicates medium values, and red indicates the highest values. The star shape denotes the optimal geometries, and the hollow square denotes the cuboid geometry.

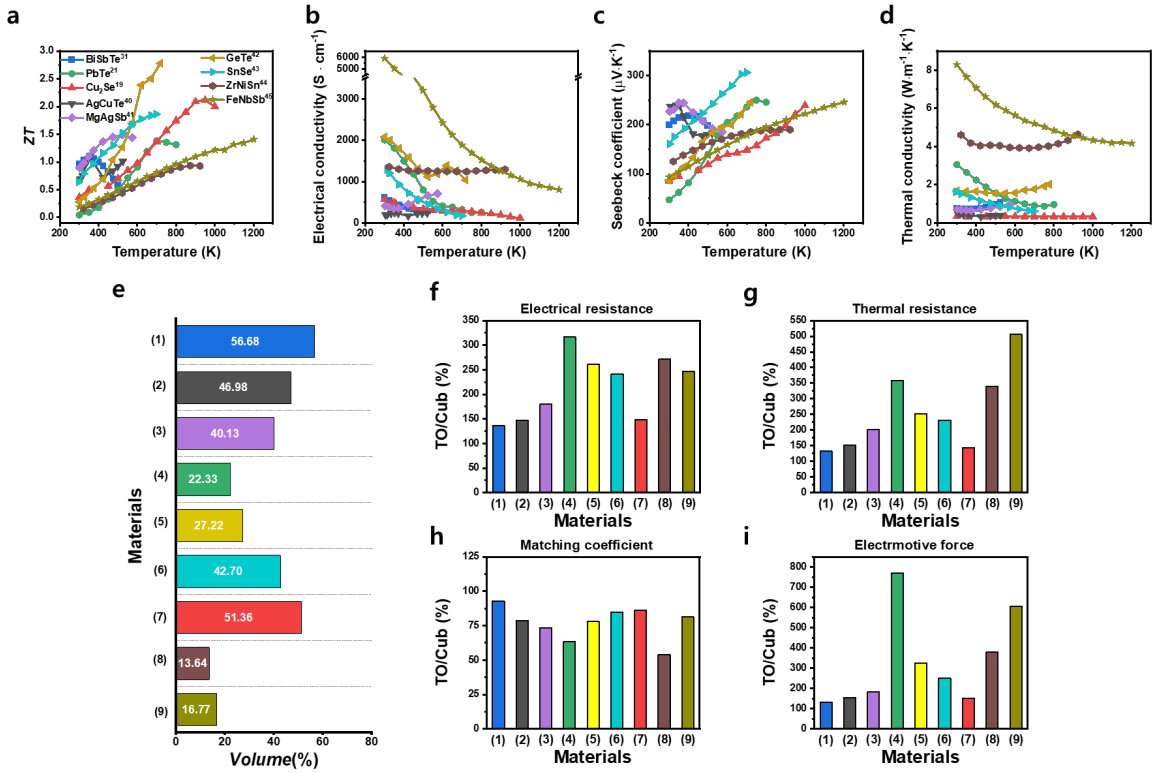

Supplementary Fig. 6 | Comparative TO results for nine distinct material properties. a–d, Temperature-dependent *ZT* (**a**), electrical conductivities (**b**), Seebeck coefficients (**c**) and thermal conductivities (**d**) of the different nine materials. Material properties were adopted from Ref. 19, 21, 31 and 40–45. **e–h** Analysis of the optimal designs under a fixed hot-side heat flux with convective cooling: volume fraction of each optimized geometry relative to the design domain (**e**), and ratios of electrical resistance (**f**), thermal resistance (**g**), matching coefficient (**h**), and electromotive force (**i**) compared with those of a cuboid-shaped leg.

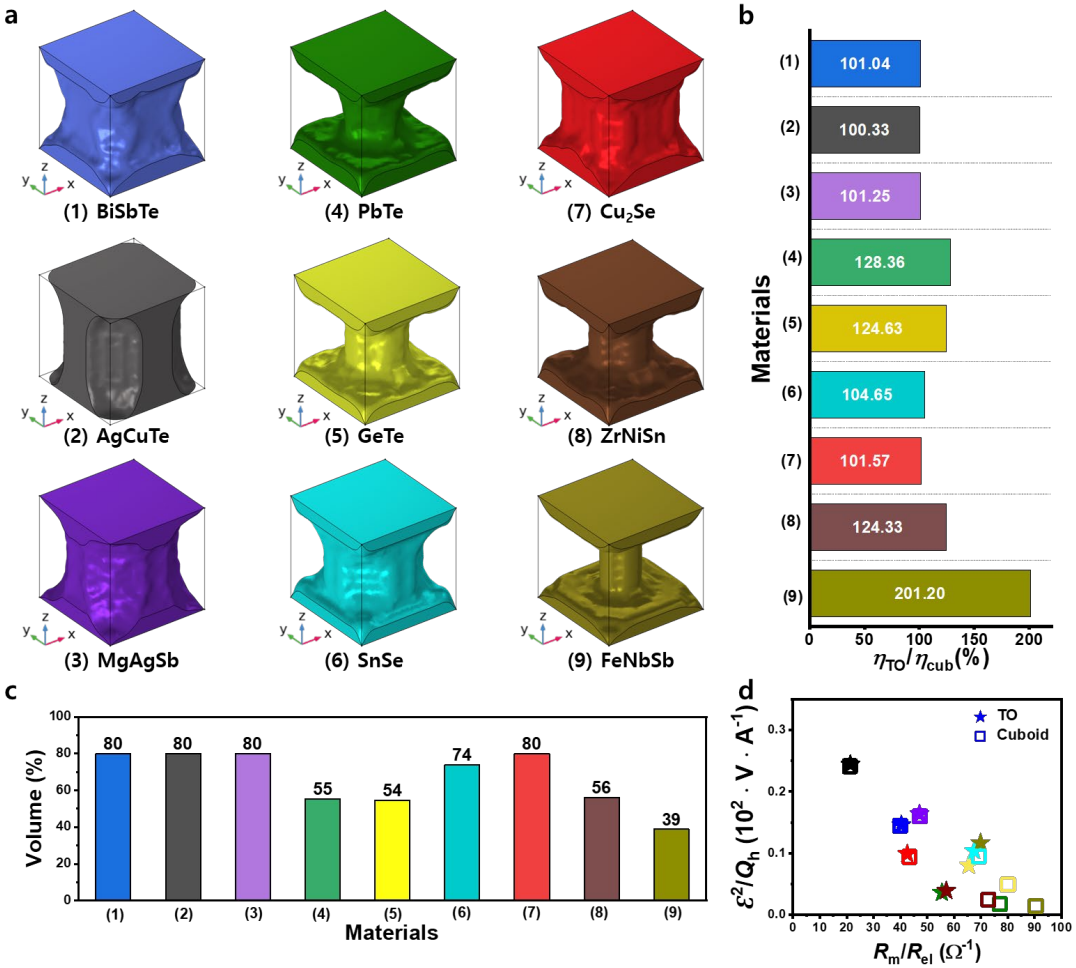

Supplementary Fig. 7 | Optimal designs under fixed-temperature conditions for nine distinct material sets. a, Optimized geometries derived from topology optimization using nine different material properties, with fixed tempearture at the hot and cold sides. **b**, η enhancement relative to a cuboid of equivalent material volume from **a**. **c,** volume fraction of each optimized geometry relative to the design domain. **d**, Analysis of η enhancement for the optimal designs from **a**. Star symbols denote the topology-optimized designs, hollow squares denote the reference cuboid, and the colors (in nine variations) match those in a, indicating the corresponding set of material properties.

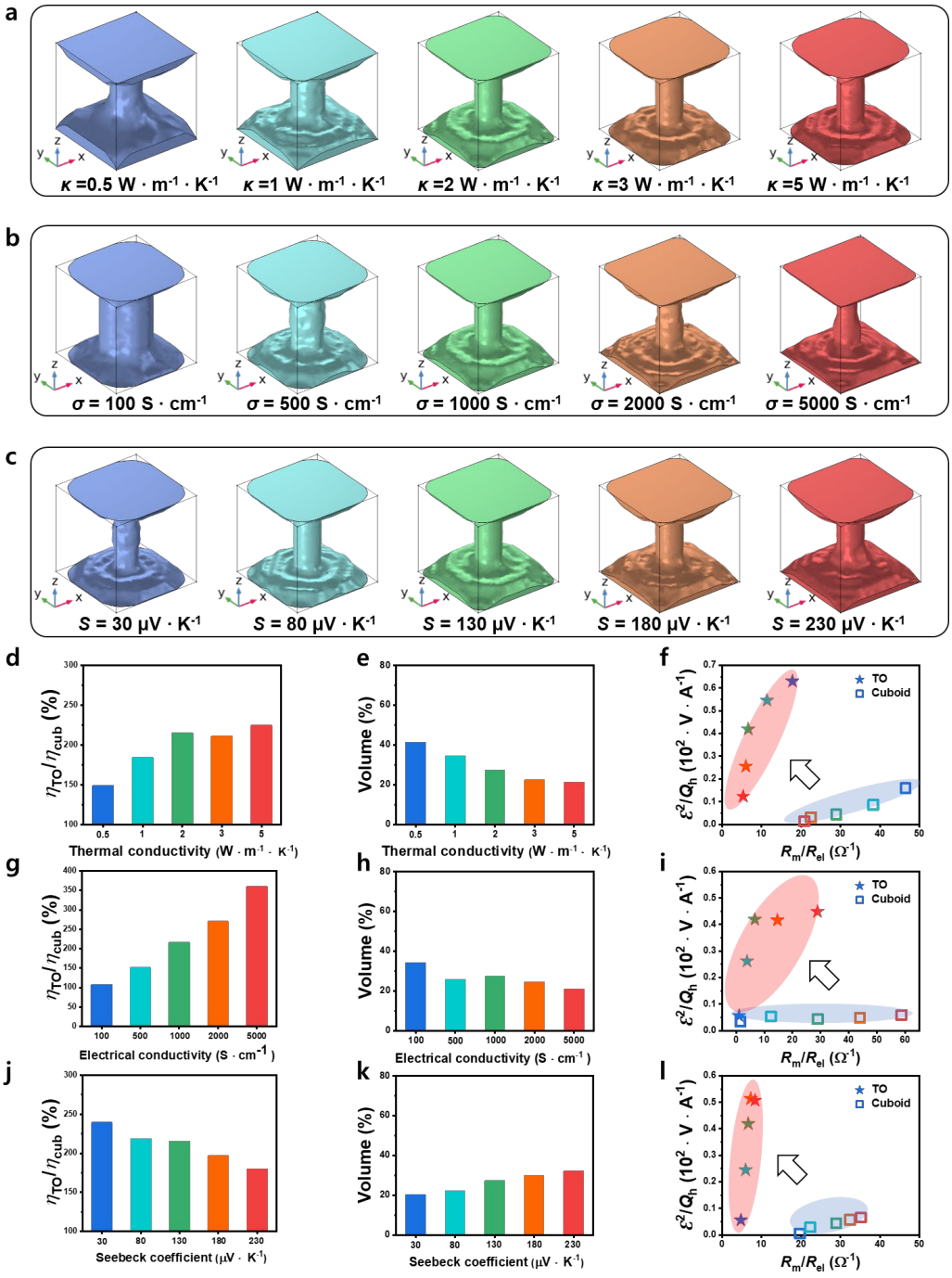

Supplementary Fig. 8 | Influence of thermoelectric property variations on optimal designs. **a**–**c**, Optimized geometries derived from TO under constant-property assumptions, varying k (**a**), σ, (**b**), and S (**c**).**d**–**l,** Numerical simulations of the corresponding optimized designs from **a** (**d**–**f**), **b** (**g**–**i**), and **c** (**j**–**l**). In each trio, the first panel (**d**, **g**, **j**) shows the percentage increase in η compared to a cuboid TE leg, the second (**e**, **h**, **k**) provides the volume percentage of the optimal design relative to the initial domain, and the third (**f**, **i**, **l**) details the analysis of η under these conditions. The colors of the symbols in **d**–**l** match those of the geometries in **a**–**c**, indicating the corresponding sets of thermoelectric properties. The star shape denotes the optimal geometries, and the hollow square denotes the cuboid geometry.

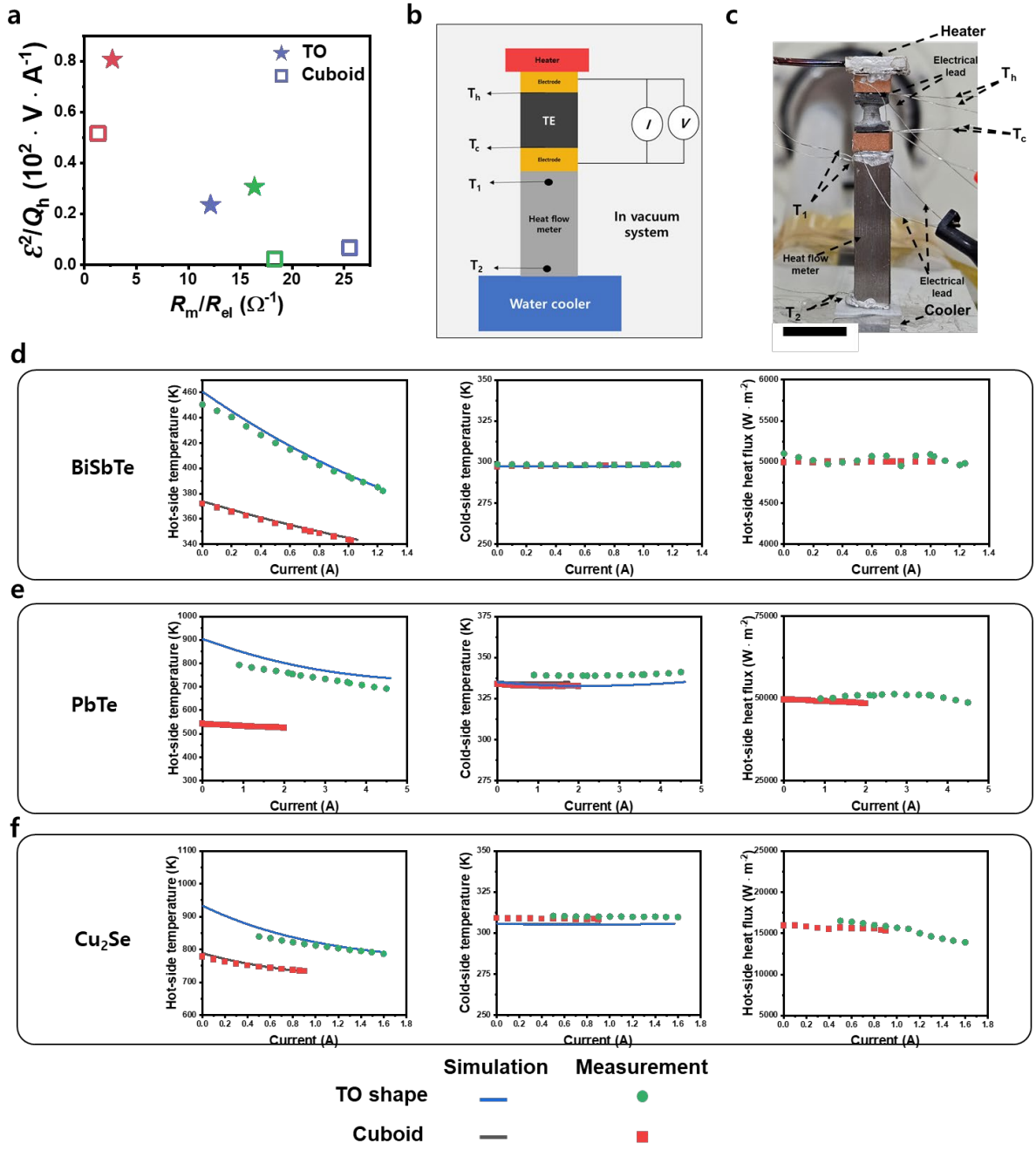

Supplementary Fig. 9 | Experimental validation of Integrated optimal designs of TE materials. a, Analysis of the η enhancement achieved through optimal designs. Blue, green, and red correspond to BiSbTe, PbTe, and Cu_2Se, respectively, while the star symbols denote the optimized geometry and the hollow squares denote the cuboid reference. **b**, Schematic illustration for measurement set-up. **c**, Photograph of the measurement setup shown in **b**. The scale bar is 10 mm. **d–f**, Measured T_h, T_c and Q_h of BiSbTe (**d**), PbTe (**e**) and Cu_2Se (**f**). The solid line represents simulation results, the green and red circles denote the properties of the optimized geometries and cuboid, respectively

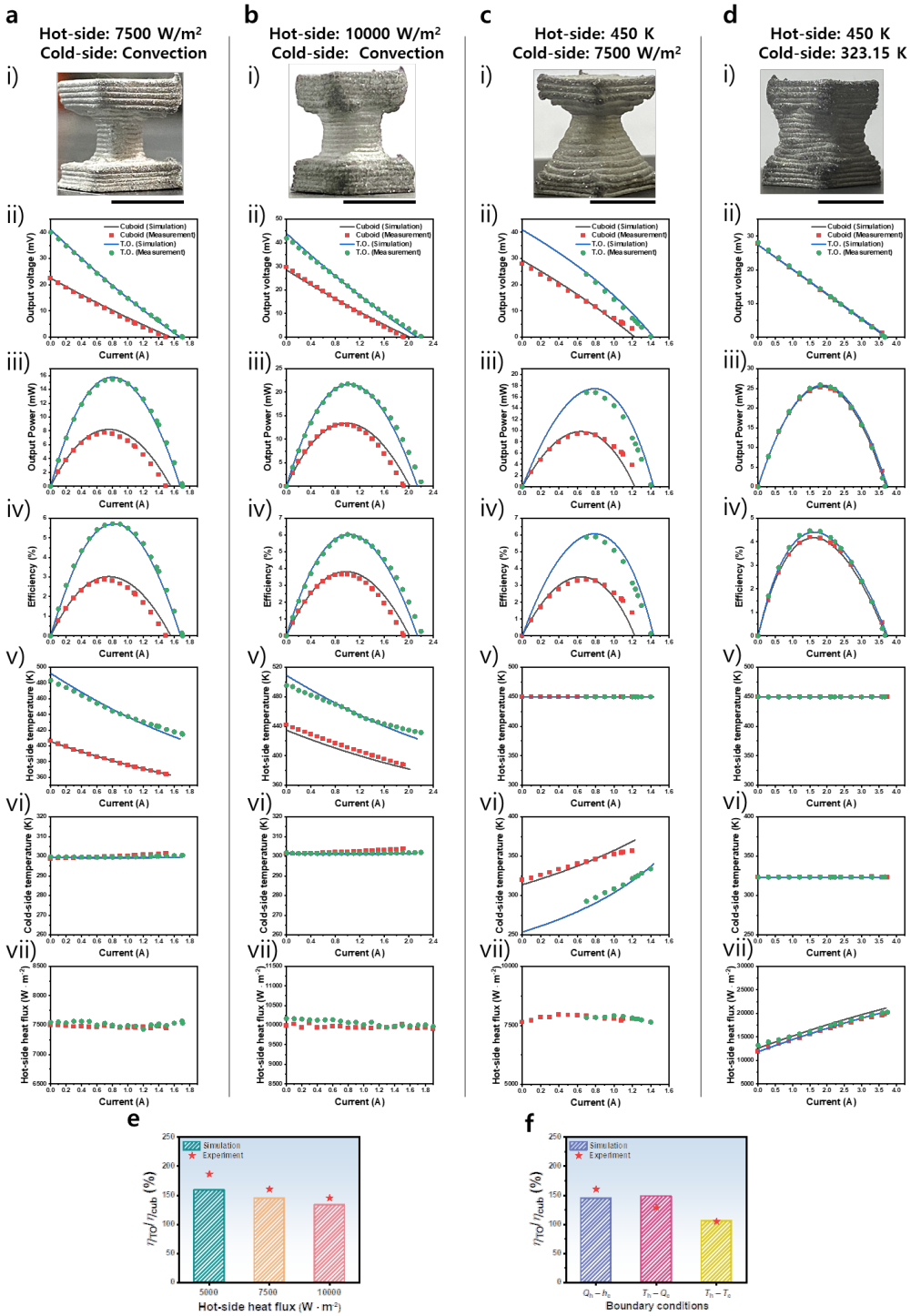

Supplementary Fig. 10 | Experimental validation of different systems. a–d, Experimental results of BiSbTe samples for different system setups. In **a** and **b**, the Q_h is fixed at 7,500 and 10,000 W m^{-2} , respectively. In **c**, the T_h is fixed while the Q_c is 7,500 W m^{-2} . In **d**, both T_h and T_c are fixed at 450 K and 323 K, respectively. For each panel (**a–d**), subpanels (i–vii) show: (i) a photograph of the optimal design, (ii) output voltage, (iii) output power, (iv) η, (v) T_h, (vi) T_c, and (vii) hot-side heat flux, respectively. The scale bar is 5 mm. **e**,**f**, the percentage of η enhancement compared to the cuboid as Q_h (**e**) and thermal boundaries (**f**).

References

1 Ryu, B. et al. Best thermoelectric efficiency of ever-explored materials. *iScience* **26**, (2023).

2 Bjørk, R. The universal influence of contact resistance on the efficiency of a thermoelectric generator. *J. Electron. Mater.* **44**, 2869–2876 (2015).

3 Choo, S. et al. Cu_2Se-based thermoelectric cellular architectures for efficient and durable power generation. *Nat. Commun.* **12**, 3550 (2021).

4 Ma, X., Shu, G., Tian, H., Xu, W. & Chen, T. Performance assessment of engine exhaust-based segmented thermoelectric generators by length ratio optimization. *Appl. Energy* **248**, 614–625 (2019).

5 Attar, A., Lee, H. & Snyder, G. J. Optimum load resistance for a thermoelectric generator system. *Energy Convers. Manag.* **226**, 113490 (2020).

6 Lesage, F. J. & Pagé-Potvin, N. Experimental analysis of peak power output of a thermoelectric liquid-to-liquid generator under an increasing electrical load resistance. *Energy Convers. Manag.* **66**, 98–105 (2013).

7 Tan, Y., Meegahapola, L. & Muttaqi, K. M. A review of technical challenges in planning and operation of remote area power supply systems. *Renew. Sustain. Energy Rev.* **38**, 876–889 (2014).

8 Khezri, R., Mahmoudi, A., Aki, H. & Muyeen, S. Optimal planning of remote area electricity supply systems: Comprehensive review, recent developments and future scopes. *Energies* **14**, 5900 (2021).